

Intent-Based Orchestration in Open RAN: An ns-3 Simulation Framework

Pouya Agheli and Grégoire Lefebvre
Orange Research, Grenoble, France

Abstract—This paper presents an extensible ns-3-based simulation framework for evaluating intent-based, semantics-aware control in Open RAN architectures. The framework integrates external Radio Access Network (RAN) Intelligent Controller (RIC) components and supports fine-grained control via internal distributed applications (dApps), enabling intent-based RAN orchestration across different timescales while maintaining standardized network behavior. As an illustrative use case, we implement an intent-based dApp for radio resource management (RRM) under realistic observability constraints. The scheduling problem is formulated using realistic key performance measurements (KPMs) available to dApps, together with a newly introduced Intent Satisfaction Score (ISS), which quantifies the delivery of intent-relevant information by combining distortion- and perception-oriented measures. Simulation results show that intent-based RRM can improve ISS while significantly reducing radio resource usage and computational overhead, at the cost of a moderate reduction in packet delivery ratio and throughput.

Index Terms—Open RAN, Intent-Based RRM, Simulation

I. INTRODUCTION

The rapid growth of cyber-physical systems demands real-time, reliable, and resource-efficient information exchange. To scale while conserving limited communication resources, modern networks are shifting from intent-agnostic, maximalist designs toward intent-based, minimalist approaches that communicate *only* information relevant to predefined intents. Under this philosophy, intent-based, semantics-aware communication has emerged as a paradigm for improving communication effectiveness and efficiency by judiciously using communication and computation resources.

This paradigm is commonly motivated by Weaver’s extension of Shannon’s theory [1], which distinguishes technical, semantic, and effectiveness levels of communication. While conceptually useful, these distinctions blur in practice, where semantic representation and effectiveness-driven adaptation become tightly coupled. Consequently, the semantic and effectiveness layers can be viewed as a unified service management and orchestration layer operating alongside the traditional protocol stack. This layer coordinates application-level functions—such as message compression, feature extraction, and embedding generation—while also directing resource allocation in the Radio Access Network (RAN), enabling a full-stack redesign tailored to intent-based, semantics-aware communication. More broadly, this framework aligns with the principles of Intent-Based Networking (IBN) automation,

which encompasses intent-related functions such as intent profiling, activation, and assurance [2]. While conventional IBN primarily operates at higher layers and longer control-loop timescales, semantics-aware communication extends intent realization deeper into the communication process by jointly adapting application-level operations and RAN behavior.

Open RAN architecture provides a natural foundation for this vision by introducing openness, disaggregation, and programmability into the RAN. By separating hardware and software and supporting intelligent control across multiple timescales, it facilitates the integration of intent-based, semantics-aware functionality throughout the protocol stack. O-RAN Alliance specifications [3] position the RAN Intelligence Controller (RIC) as the central platform for non-real-time (non-RT) and near-real-time (near-RT) control through modular RAN applications (rApps) and extended applications (xApps). However, the control-loop latency of the standard RIC architecture limits real-time decision-making and responsiveness to rapidly changing intents. Recent extensions [4]–[6] introduce distributed applications (dApps) that move intelligence closer to lower Open RAN nodes. This enables shorter control loops, reduced signaling overhead (up to 3.57 times [4]), and provides granular access to local network-state information, such as per-packet information and raw I/Q samples. This distributed intelligence supports edge-optimized artificial intelligence (AI) and flexible, software-based RAN adaptation, enabling real-time, intent-based decision-making in response to network dynamics.

The ns-3 simulator provides a near-realistic simulation environment for evaluating Open RAN systems compliant with 3rd Generation Partnership Project (3GPP) standards [7], widely used for Long-Term Evolution (LTE) and 5G New Radio (NR) research. Nevertheless, ns-3 is primarily developed in C++, with RAN operations implemented as native components, which makes it difficult to integrate Open RAN elements—such as RICs and intelligent control applications. Supporting flexible and programmable Open RAN control requires either interfacing with external control modules or redesigning internal components, the latter often limiting extensibility in practice. This gap underscores the need for modular, realistic Open RAN simulation frameworks that support the incorporation of intent-based, semantics-aware orchestration.

A. Related Works

Several studies in the ns-3 and Open RAN literature have explored integrating machine learning (ML)- or AI-based ex-

This research was funded in part by the Agence Nationale de la Recherche (ANR) under the ANR-24-IAS1-0002-02 COMSEMA project.

ternal control components into network simulators, often using frameworks such as ns-O-RAN [8]. The primary objective of these efforts is to enhance flexibility in RAN operations, especially in Medium Access Control (MAC) scheduling, through data-driven optimization. Representative examples include [9] and [10], which integrate external ML- and AI-empowered radio resource management (RRM) controllers with ns-3 using the ns3-gym framework [11]. However, they do not support intent-based orchestration, primarily focus on proposing data-driven solutions for isolated RAN operations, and lack dApp integration, thereby limiting their applicability to near-RT or higher-layer control.

Further research explores the convergence of Open RAN and semantic communications through intelligent RRM [12]–[15], addressing topics such as sub-millisecond scheduling, joint radio and compute slicing, RIC-enabled intelligence, and AI-driven satellite–terrestrial coordination. Despite reported gains, the broader impact remains constrained by AI-induced reasoning errors, high energy consumption, and the lack of a realistic, modular, and reproducible Open RAN simulation framework that supports intent-based, real-time control.

B. Contributions

We develop an open-source¹, reproducible simulation framework extending ns-3 for realistic evaluation and benchmarking of intent-based orchestration in Open RAN, which is released as **ib-ORAN**. The framework integrates two sets of Python-based control modules—local dApps and external RIC components—with the ns-3 network environment via a high-performance shared-memory interface, enabling coordinated control across multiple timescales while adhering to Open RAN architectural principles and 3GPP standards. Leveraging the ns3-ai module [16], the proposed design enables an efficient interaction between the C++ simulation core and Python-based control logic, achieving 50–100 times lower latency [16] than socket-based alternatives such as ns3-gym used in [9] and [10]. This capability supports the realistic implementation of fine-grained, real-time RAN control mechanisms.

Using this framework, we propose an update to the Open RAN logical architecture to support intent-based orchestration, detail the resulting system structure and data flows, and implement a dApp for intent-based RRM as an initial use case for validating simulator operation. We define an Intent Satisfaction Score to capture intent-dependent semantic relevance under practical observability constraints and formulate the corresponding RRM problem based on limited low-level measurements available to local dApps. Simulation results compare representative scheduling strategies and identify which realistic metrics best reflect intent-relevant performance.

II. OPEN RAN ARCHITECTURE WITH INTENT SUPPORT

The O-RAN Alliance classifies Open RAN nodes as central, distributed, and radio units (O-CU, O-DU, and O-RU) [3]. Although the O-RAN architecture is inherently modular

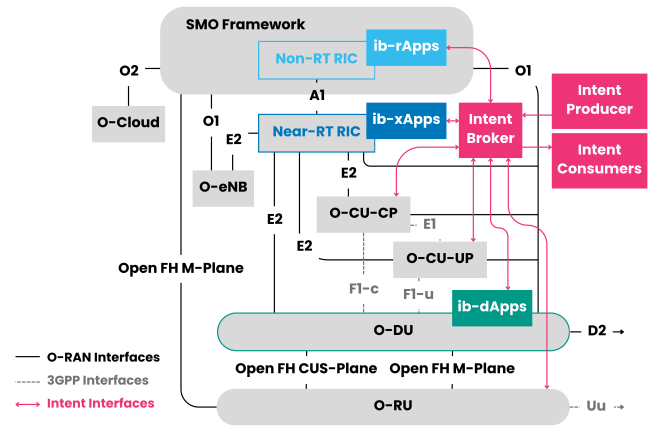


Fig. 1. Open RAN logical architecture with intent support.

and software-driven, supporting intent-based, semantics-aware control requires additional functional and interfacing elements. Addressing it involves gradually enhancing mechanisms within the service management and orchestration (SMO) framework, non-RT and near-RT RICs, and lower-layer dApp controllers.

Two complementary enhancements are needed. First, new architectural elements must be defined to issue, manage, and distribute timely intents and requirements across Open RAN nodes. Second, native control components must be extended to support the execution of intent-based, semantics-aware control policies by hosting *intent-based rApps* (*ib-rApps*), *xApps* (*ib-xApps*), and *dApps* (*ib-dApps*). These enhancements should avoid introducing bulky components, excessive computational overhead, or disruptions to architectural modularity. Existing studies support elements of this direction (see [13] and [12]), though the approach proposed here distinguishes itself by integrating intent-based orchestration across multiple control layers within a unified, deployable architecture. Fig. 1 illustrates the resulting architecture, which augments native Open RAN and 3GPP-compliant elements with components that explicitly support intent-based orchestration.

The *Intent Broker* plays a central role in the proposed architecture. Serving as a coordination hub, it connects the Open RAN system to external entities such as the *Intent Producer*, which supplies high-level intents and semantic metadata for service data units, and *Intent Consumers*, which indirectly exploit this information to support coordinated operations. The Intent Broker aggregates incoming intent information, distributes global intents towards architectural layers, translates them into actionable instructions for *ib-rApps* and *ib-xApps*, and ensures consistent interpretation across control modules. It also dispatches intents directly to *ib-dApps*, bypassing purely syntactic processing and inter-node control signaling, thereby enabling timely and fine-grained local decision-making.

These interactions rely on dedicated *Intent Interfaces* that connect intent-aware components with native elements and expose controlled access to external policy makers or consumers. The interfaces operate bidirectionally, allowing control com-

¹Code available at <https://github.com/Orange-OpenSource/ns3-iboran>.

dApp submodule to return control actions to the E3 agent via E3 CONTROL messages, which are subsequently enforced at the MAC scheduler (see [6] for further details).

The second class of inputs comprises higher-level control policies and configuration directives issued by ib-xApps at a coarser timescale of 10 TTIs.⁴ These directives are conveyed to the E3 agent over the E2 interface using a custom, non-standard E2 Service Model for dApp (E2SM-DAPP) [6], transported via RIC CONTROL messages. An internal E2–E3 bridge enables the E3 agent to interpret these directives and forwards them to the ib-dApps. Conversely, ib-dApps generate enrichment information—such as scheduling context or allocation summaries—which is shared with ib-xApps via the same E2SM-DAPP, translated by the E2–E3 bridge into E2SM-DAPP indication payloads, and then delivered to ib-xApps as RIC REPORT messages.

To reduce signaling overhead and control-channel load, the exchange of report and control messages between the eNodeB dApp submodule and the near-RT RIC module occurs at a coarse periodicity of 10 TTIs, since the external control loop is the primary bottleneck. Accordingly, we can define Δ_{dApp} as an integer divisor of the near-RT control period. This design choice aligns fine-grained dApp updates with coarser near-RT RIC cycles, ensuring that E2- and E3-agent inputs are available at well-defined synchronization points.

Based on the most recent local measurements, higher-level directives from ib-xApps, and time-varying intents from the Intent Broker, ib-dApps perform fine-grained decision-making every Δ_{dApp} TTIs. The resulting control actions are immediately enforced by updating the MAC scheduler operation.

2) *RIC modules*: The near-RT RIC module performs coarse-grained decision-making based on two sets of input reports: higher-level measurements from the eNodeB MAC and RLC layers, and decision summaries generated by the eNodeB dApp submodule. The first set is reported over the E2 interface using the E2SM-KPM and delivered via its REPORT service as RIC REPORT messages at a periodicity of 10 TTIs. The second set follows the E2SM-DAPP specifications (see Section III-B1) and is conveyed in separate RIC REPORT messages that carry E2SM-DAPP-defined payloads.

Based on these report streams and timely intents from the Intent Broker, the near-RT RIC derives higher-level control policies and optimization directives every 10 TTIs. In addition, the non-RT RIC supports near-RT decision-making by providing long-term policy guidance, optimization objectives, and, where applicable, trained AI/ML models via the A1 interface.

Coarse-grained control policies and configuration directives generated by ib-xApps are delivered to the dApp submodule over the E2 interface using the E2SM-DAPP control semantics and transported in RIC CONTROL messages. These directives are then forwarded through the internal E2–E3 bridge to ib-dApps, where they guide local control logic responsible for fine-grained MAC scheduling decisions. Consistent with the

⁴We consider ib-xApps to operate at the minimum supported near-RT control period of 10 ms, in line with Open RAN specifications and the discrete-event execution model of ns-3.

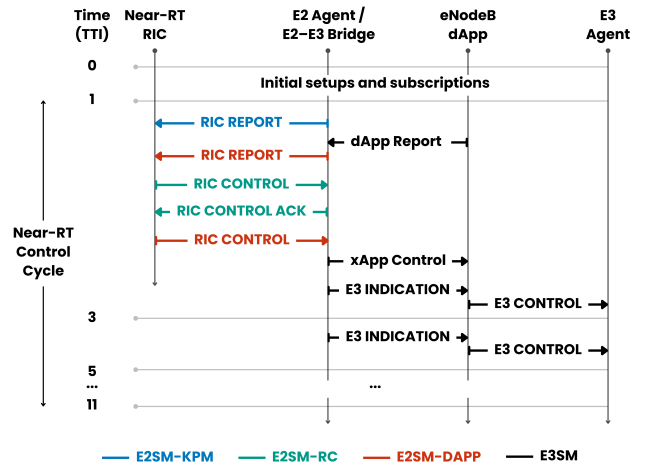


Fig. 3. Time-based message exchange among the near-RT RIC, eNodeB dApp submodule, and interfaced E2 and E3 agents.

Open RAN framework, the near-RT RIC may also issue control decisions directly to RAN operations based on the E2SM-RC and its CONTROL service, delivered by RIC CONTROL messages. Such actions are enforced immediately at the MAC scheduler, bypassing longer-term policy mediation.

Fig. 3 provides a time-based overview of information exchanges among simulator components during a single near-RT control cycle, detailing the associated service models and message types for each interaction. In this configuration, we set $\Delta_{dApp} = 2$, such that one near-RT control cycle of 10 TTIs encompasses five consecutive local control loops. Moreover, Table I summarizes the message payloads exchanged under each service model. Here, RNTI, CQI, QCI, and MCS denote the radio network temporary identifier, channel quality indicator, quality of service class identifier, and modulation and coding scheme, respectively.

IV. IMPLEMENTATION OF INTENT-BASED RRM

In this section, we discuss the implementation of intent-based RRM, encompassing user selection and radio resource allocation. At intervals of Δ_{dApp} TTIs, the ib-dApp selects one or more UEs using a scheduling mechanism and allocates their required radio resources in accordance with high-level directives and constraints issued by ib-xApps.

The smallest allocable unit of radio resources is the Physical Resource Block (PRB). According to 3GPP LTE-A specifications, uplink transmissions require contiguous PRB allocations per carrier component due to DFT-spread OFDM, whereas contiguity is not mandatory on the downlink. In the developed simulation framework, downlink allocation follows Type-0 resource allocation, in which the system bandwidth is partitioned into Resource Block Groups (RBGs), each comprising a fixed number of PRBs determined by the total system bandwidth.

A. Key Performance Indicators

To evaluate the performance of the network in handling traffic across different input data formats, the simulator supports

TABLE I
INFORMATION EXCHANGED OVER THE E2 AND E3 INTERFACES.

Service Model	Message Type	Message Payload
E2SM-KPM	RIC REPORT	Aggregated and per-UE KPMs from the MAC and RLC layers (e.g., number of active UEs, resource utilization, throughput, latency, buffer level, CQI-related indicators, etc.).
E2SM-RC	RIC CONTROL	High-level radio control directives and policy configurations (e.g., scheduling constraints, prioritization rules, admission control decisions, link adaptation policies, etc.).
E2SM-DAPP	RIC REPORT	Total number of served UEs, allocated resources, system load handled, and per-UE information (e.g., average throughput, packet delay, total bytes served, etc.).
E2SM-DAPP	RIC CONTROL	Resource budget, scheduling approaches, skipping specific frames or UEs, etc.
E3SM	E3 INDICATION	Number of active UEs, available resources, current subframe number, link direction, and per-UE information (e.g., RNTI, CQI, QCI, buffer level, criticality, etc.).
E3SM	E3 CONTROL	RNTI of selected UEs, per-UE resource allocation map, MCS, etc.

standard KPIs, including packet delivery ratio (PDR), throughput, latency, and jitter. Additionally, it allows the definition of context- or semantics-aware metrics tailored to specific data formats and applications. Without loss of generality, in this work, both uplink and downlink traffic are generated from user-specific, labeled image files.

To quantify the extent to which network transmissions satisfy the underlying intent, we introduce the *Intent Satisfaction Score (ISS)* metric, denoted by \mathcal{S}_I and defined as⁵

$$\mathcal{S}_I = h_I(\mathcal{F}), \quad \mathcal{F} = \alpha f_0 + \beta f_1 + \gamma f_2, \quad (1)$$

where \mathcal{F} is the fidelity score composed of semantic, content, and structural fidelity components, f_0 , f_1 , and f_2 , respectively, each taking values in $[0, 1]$. Also, $\alpha, \beta, \gamma \in [0, 1]$ show weighting coefficients that satisfy $\alpha + \beta + \gamma = 1$. The fidelity score combines distortion- and perception-oriented measures, consistent with established principles of semantic communication [17]. Specifically, f_0 captures perception-related (semantic) fidelity, f_2 reflects distortion-related fidelity, and f_1 serves as a hybrid measure that integrates both aspects.

An intent-based activation function $h_I : [0, 1] \rightarrow [0, 1]$ maps the fidelity score \mathcal{F} to the ISS based on its relevance to the underlying intent. For intent-relevant data flows with $\mathcal{F} \geq \mathcal{F}_{\min}$, we set $h_I(\mathcal{F}) = \mathcal{F}$, where $\mathcal{F}_{\min} = 0.2$ is the minimum acceptable fidelity⁶; otherwise, $h_I(\mathcal{F}) = 0$.

1) *Semantic fidelity*: To derive semantic fidelity between a transmitted image and its reconstruction, we use the Contrastive Language–Image Pretraining (CLIP) model [18]. CLIP is first applied to the entire image to obtain a global similarity score. The image is then divided into equal-sized patches (in this work, 16 patches arranged in a 4×4 grid), and semantic fidelity is evaluated for each patch separately.⁷ Therefore, we have

$$f_0 = \frac{g_s}{2} \cdot (f_{0,\text{global}} + f_{0,\text{patch}}), \quad (2)$$

where $f_{0,\text{global}}$ and $f_{0,\text{patch}}$ denote the global and average patch-level semantic fidelity, respectively. A spatial coverage

⁵To the best of our knowledge, no globally accepted metric exists for this purpose. The proposed formulation serves as a baseline, while the simulator remains agnostic to any specific ISS definition.

⁶This threshold can be adjusted depending on the user application or intent.

⁷Patch-level assessment captures localized semantic degradations that may not be reflected in the global similarity score.

factor g_s is also introduced, defined as the fraction of patches whose similarity score exceeds a prescribed threshold. In this work, the similarity threshold is arbitrarily set to 80%.

2) *Content fidelity*: To quantify content fidelity, we partition both transmitted and reconstructed images into 16-pixel blocks and compare their intensity variance. Blocks in the transmitted image with variance above a threshold are considered content-bearing. Content fidelity is measured as the fraction of these blocks that retain comparable variance after reconstruction. A variance threshold of 10 is adopted, which effectively distinguishes informative regions from visually flat areas in grayscale images at the considered resolution.

3) *Structural fidelity*: Assessing structural fidelity, we employ the single-scale Structural Similarity Index (SSIM) [19], which measures local similarity between a transmitted image and its reconstruction by accounting for luminance, contrast, and structural information at the pixel level.⁸

All metrics are computed after resizing the transmitted and reconstructed images to a common resolution of 224×224 pixels. The content and structural fidelity components (f_1 and f_2) are evaluated on grayscale images.

4) *Intent definition*: In this work, intents correspond to requests for specific object identities (IDs) within a labeled image dataset. Each image is annotated with the IDs of the objects it contains, which may include one or more. During every simulation episode, each UE randomly selects an image for uplink transmission while the remote host independently selects images for downlink transmission to the UEs. At the beginning of the episode, the Intent Producer randomly activates one object ID as the current intent. The fidelity score \mathcal{F} is therefore deemed intent-relevant only if the transmitted image contains the requested object ID. Otherwise, the transmission does not contribute to the ISS through $h_I(\mathcal{F})$, regardless of its visual fidelity.

B. Problem Formulation

A natural approach to designing the ib-dApp for RRM is to formulate an optimization problem that maximizes a weighted combination of standard KPIs and the ISS through long-term, end-to-end objectives. However, such a formulation

⁸More advanced perceptual fidelity metrics, such as SSIMULACRA 2 [20], exist, but their conceptual complexity falls outside the scope of this work.

rests on strong assumptions about the stability of intent and the feasibility of defining a system-level objective for a low-level control loop operating under real-time, time-varying network dynamics. In practice, these assumptions are difficult to meet. Furthermore, in an ns-3 implementation compliant with 3GPP standards, the eNodeB dApp submodule primarily observes fine-grained network-state measurements from the MAC and RLC layers at the eNodeB and the UEs. Since intent satisfaction can only be evaluated after complete image transmission and reconstruction, the ib-dApp cannot access the fidelity score—and hence the ISS—in real time.

As a result, RRM decisions rely on information conveyed through E3 INDICATION and xApp Control messages (see Section III), together with intent-relevance indicators such as side information and context-aware criticality. Under these constraints, the RRM objective combines intent relevance with available low-level, real-time KPMs, including CQI, QCI, and buffer level. We therefore adopt a grant-based, buffer-aware resource allocation strategy in which each selected UE is assigned sufficient downlink or uplink radio resources to drain its buffer during its scheduled TTIs. The required number of PRBs (or RBGs) is determined from the UE’s CQI, MCS, and buffer level, looking up predefined mapping tables specified in the 3GPP LTE-A standards [21].

Consequently, the RRM problem reduces to a user-selection problem driven by the estimated resource demands, low-level KPMs, and intent-relevance indicators observable at the dApp submodule. We formulate the resulting scheduling task as a classical knapsack problem [22]:

$$\begin{aligned} \mathcal{P} : \quad & \max_{\{x_i \in \{0,1\}\}_{i=0}^n} \sum_{i=1}^n v_i(\kappa_i) x_i \\ \text{s.t.} \quad & \sum_{i=1}^n b_i x_i \leq B_{\max}, \end{aligned} \quad (3)$$

where $n \geq 0$ shows the number of active UEs (i.e., UEs with pending data) during a scheduling interval of Δ_{dApp} TTIs. Also, $b_i > 0$ denotes the estimated number of PRBs (or RBGs) required by the i -th UE for uplink (or downlink) transmission, and B_{\max} represents the total radio resources available for *new* transmissions⁹ in the current scheduling interval.

Moreover, $v_i, \forall i$, is the scheduling utility associated with selecting the i -th UE. This utility is determined from a chosen KPM, denoted by κ_i , which depends solely on information available to the ib-dApp, such as intent-relevance indicators and low-level measurements (e.g., CQI, QCI, and buffer level). In Section V, we identify which uplink and downlink KPMs best align with ISS-related performance under the given observability constraints.¹⁰

C. Scheduling Algorithm

Regardless of the specific KPM used to model the scheduling utility, we tailor a greedy density-based UE selection

⁹A portion of resources is dynamically reserved for HARQ retransmissions.

¹⁰Although no single KPM fully captures intent satisfaction, this analysis provides practical guidance on proxy metrics that best correlate with ISS under realistic deployment conditions.

TABLE II
NS-3 CONFIGURATION PARAMETERS.

Parameter	Value	Parameter	Value
Simulation area	500 × 500 m ²	Simulation episode	10 s
Number of UEs	10	Number of eNodeBs	1
Uplink packet size	1400 bytes	Downlink packet size	1400 bytes
Uplink source rate	100 kbps	Downlink source rate	200 kbps
Uplink L4 protocol	UDP	Downlink L4 protocol	UDP
Uplink EARFCN*	20750	Downlink EARFCN	2750
Uplink PRBs	100	Downlink RBGs	25
Downlink RBG size	4 PRB	System bandwidth	20 MHz
Per-PRB bandwidth	180 kHz	Per-RBG bandwidth	720 kHz
LTE-A TX mode	TM2 [21]	P0 nominal PUSCH	−96 dBm
UE TX power	[−40, 23] dBm	eNodeB TX power	46 dBm

*EARFCN: 3GPP-defined index identifying the LTE-A carrier frequency [23].

algorithm to solve problem \mathcal{P} . Each UE i is assigned a utility density $\rho_i = v_i(\kappa_i)/b_i$, defined as the ratio between its utility and estimated radio resource requirement. Active UEs are sorted in descending order of ρ_i and selected iteratively until the available resources are depleted. This algorithm exhibits time and space complexities of $\mathcal{O}(n \log n)$ and $\mathcal{O}(n)$, respectively, enabling low-latency decision-making with reduced computational overhead compared to conventional alternatives such as dynamic programming or exhaustive combinatorial search. These properties make the greedy density-based strategy suitable for real-time RRM in ib-dApps. Nonetheless, the method is generally suboptimal for the formulated knapsack problem and achieves optimality only in the special case where all UEs require the same amount of resources.

V. SIMULATION RESULTS

In this section, we validate the performance of the developed ns-3-based Open RAN simulator, compliant with 3GPP LTE-A specifications, and investigate the functionality of the designed ib-dApp for RRM. We compare multiple UE selection strategies using different KPMs and intent-relevance indicators available within the eNodeB dApp submodule. We then identify which KPM and corresponding scheduling utility definition (see Section IV-B) best align with the ISS-based evaluation for both uplink and downlink. In this evaluation, we set $\alpha = 0.4$ and $\beta = \gamma = 0.3$ to specify \mathcal{S}_I in (1). The results are averaged over $\Delta_{\text{dApp}} \in \{1, 4, 8\}$.

We consider a scenario with 10 UEs initially distributed at random within a 500 × 500 m² area, connected to a single eNodeB with a tower height of 30 m. Each UE has a height of 1.5 m and moves at a constant speed of 3 km/h under a two-dimensional random walk mobility model, changing direction every 10 m. Large-scale propagation is modeled using the HybridBuildings propagation loss model [24] in a medium-sized urban environment, while small-scale fading follows a 3GPP-compliant trace-based Extended Pedestrian A (EPA) channel model [25]. Unless otherwise specified, the key ns-3 configuration parameters and their values are listed in Table II; all other parameters follow the default ns-3 settings.

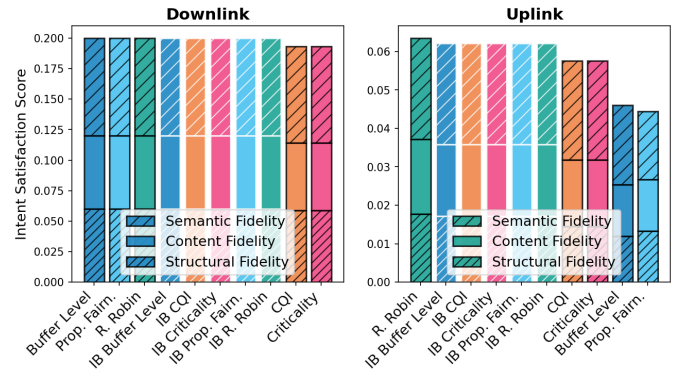
Applying the proposed greedy density-based UE selection algorithm in Section IV-C, the utility density is defined as a function of measurements available to the dApp submodule, including CQI, buffer level, and context-aware criticality¹¹, combined with proportional fairness computed from the UEs' instantaneous achievable data rate and historical throughput. Each utility definition yields a distinct greedy selection strategy. Additionally, conventional round-robin scheduling is adopted as a baseline. For each strategy, an intent-based variant (denoted IB) is evaluated. At each control interval, UEs are partitioned into relevant and irrelevant groups based on whether their content object ID matches the requested intent. Relevant UEs are unconditionally admitted to the candidate pool, after which irrelevant UEs are greedily admitted in order until the total resource demand reaches the available capacity.

Fig. 4 compares Open RAN performance across different intent-based and intent-agnostic UE selection strategies for the formulated RRM problem (see Section IV-B). Performance is evaluated based on the ISS metric and conventional KPIs—PDR (packet delivery ratio), throughput, and latency—for both downlink and uplink transmissions (see Figs. 4(a)–4(d)). Furthermore, to highlight the associated costs, Fig. 5 reports the average percentage of allocated PRBs and the decision time for each strategy across both uplink and downlink.

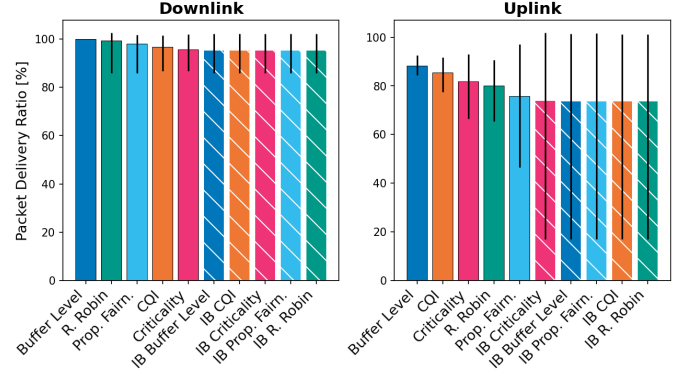
For both downlink and uplink transmissions, intent-based approaches achieve higher average intent satisfaction than their intent-agnostic counterparts, albeit at the cost of reduced PDR and throughput, as UEs are prioritized based on information relevance rather than on instantaneous network conditions. According to Fig. 4, applying intent-based UE selection increases average intent satisfaction by up to 3.3% (28.48%) on the downlink (uplink), while reducing PDR and throughput by an average of 2.75% (11.3%) and 2.8% (11.8%), respectively.

Additionally, intent-based approaches yield a 4.1% reduction in average uplink transmission latency. The primary reason is that UEs carrying relevant information are consistently prioritized within a simulation episode, ensuring timely and reliable access to transmission and retransmission opportunities, even under unfavorable channel conditions. As a result, these UEs experience reduced waiting times between successive transmission attempts. In contrast, under intent-agnostic strategies, mobile UEs may experience intermittent resource allocation due to variations in channel quality or buffer levels across multiple intervals, leading to increased latency before successful packet delivery. Nonetheless, in the downlink, the higher transmission power at the eNodeB and the lower loss probability shift the dominant factor from channel limitations to scheduling effects. In this case, intent-based prioritization increases latency by 43.1% on average, as UEs with irrelevant information may encounter long queuing delays.

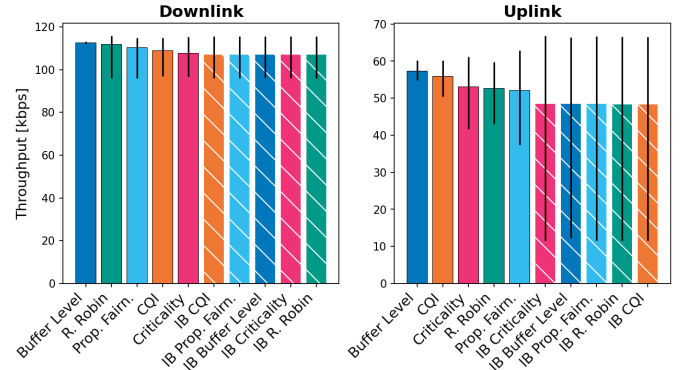
¹¹The criticality of a UE is determined by the importance of its pending packets. Each packet corresponds to a portion of an image compressed in the Portable Network Graphics (PNG) format and may contain chunks of varying importance. According to the PNG specification, the image header (IHDR) is assigned the highest criticality, followed by the palette (PLTE) and the first image data chunk (IDAT), with decreasing criticality for subsequent IDAT chunks. The image end (IEND) chunk has the lowest criticality.



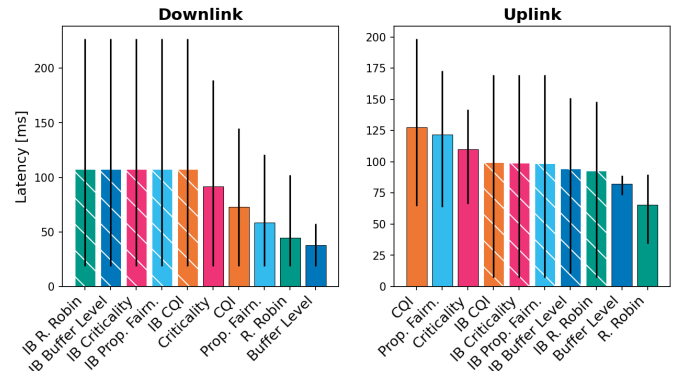
(a) ISS metric



(b) PDR metric



(c) Throughput metric



(d) Latency metric

Fig. 4. Comparison of intent-based (IB) and intent-agnostic UE selection strategies across multiple KPIs.

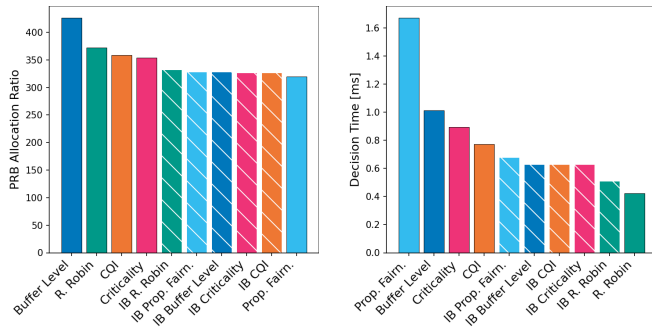


Fig. 5. Average resource usage and decision time under different UE selection strategies across uplink and downlink.

Moreover, by prioritizing UEs with intent-relevant information, intent-based strategies allocate resources more selectively. Although UEs with poor channel conditions may require more resources individually, overall resource usage is reduced by avoiding allocations to less important UEs, leading to an average 8.2%–30% reduction in resource consumption (see Fig. 5) while achieving higher intent satisfaction (see Fig. 4 (a)). This efficiency is further reflected in an average 51% reduction in decision time, mainly due to pre-selection and the smaller set of relevant candidates processed at each control interval.

VI. CONCLUSIONS AND PERSPECTIVES

This work presents an open-source, modular ns-3-based simulation framework for the realistic evaluation of intent-based, semantics-aware control in Open RAN architectures. By seamlessly integrating RIC components and enabling fine-grained, real-time control through dApps compliant with 3GPP LTE-A specifications, the framework supports systematic experimentation with intent-based orchestration across multiple timescales. As a use case, we implement an intent-based dApp for RRM and introduce the Intent Satisfaction Score (ISS) metric to quantify the delivery of intent-relevant information by combining distortion- and perception-oriented measures.

Simulation results demonstrate the framework’s capability to evaluate multidimensional performance across intent satisfaction, reliability, throughput, latency, and radio resource utilization under realistic observability constraints. The results show that intent-based RRM improves ISS while significantly reducing radio resource utilization and computational overhead, at the expense of relatively lower PDR and throughput and increased downlink latency. These findings expose inherent trade-offs between intent-dependent effectiveness and conventional network performance metrics, underscoring the importance of aligning scheduling design with deployment-specific objectives, target KPIs, and operational limitations.

Looking ahead, future research will focus on extending the framework to support 5G NR standards, incorporating predictive ML/AI-based control mechanisms, and exploring broader applications such as multi-tenant slicing. Further validation in real-world environments and the development of standardized intent-aware metrics will be essential steps toward the practical deployment of intent-based, semantics-aware control in Open

RAN systems. More broadly, the framework contributes to the development of intelligent, autonomous, and semantics-aware wireless systems envisioned in emerging 6G architectures.

REFERENCES

- [1] C. E. Shannon and W. Weaver, *The Mathematical Theory of Communication*. University of Illinois Press, Urbana, 1949.
- [2] A. Leivadreas and M. Falkner, “A survey on intent-based networking,” *IEEE Commun. Surveys Tuts.*, vol. 25, no. 1, 2022.
- [3] O-RAN Alliance, “O-RAN architecture description,” O-RAN Alliance, Technical Specification v14.01, 2025.
- [4] S. D’Oro, M. Polese, L. Bonati, H. Cheng, and T. Melodia, “dApps: Distributed applications for real-time inference and control in O-RAN,” *IEEE Commun. Mag.*, vol. 60, no. 11, 2022.
- [5] O.-R. A. N. G. R. G. (nGRG), “dApps for real-time RAN control: Use cases and requirements,” *ORAN-WG3. Tech. Spec.*, 2024.
- [6] A. Lacava, L. Bonati, N. Mohamadi, R. Gangula, F. Kaltenberger, P. Johari, S. D’Oro, F. Cuomo, M. Polese, and T. Melodia, “dApps: Enabling real-time AI-based Open RAN control,” *Computer Networks*, 2025.
- [7] G. F. Riley and T. R. Henderson, “The ns-3 network simulator,” in *Modeling and Tools for Network Simulation*. Springer, 2010, pp. 15–34.
- [8] A. Lacava, M. Bordin, M. Polese, R. Sivaraj, T. Zugno, F. Cuomo, and T. Melodia, “ns-O-RAN: Simulating O-RAN 5G systems in ns-3,” in *Proc. ACM Wkshp. ns-3*, 2023.
- [9] W. Garey, T. Ropitault, R. Rouil, E. Black, and W. Gao, “O-RAN with machine learning in ns-3,” in *Proc. ACM Wkshp. ns-3*, 2023.
- [10] H. Kim, K. Koutlia, B. Bojović, A. Ashtari, and G. Ferreira, “Evolving 5G-LENA towards 6G: Integrating AI for intelligent scheduling of multi-flow traffic,” in *Proc. Int. Conf. ns-3*, 2025.
- [11] P. Gawlowicz and A. Zubow, “ns-3 meets OpenAI Gym: The playground for machine learning in networking research,” in *Proc. ACM Int. Conf. Model., Anal. Simul. Wireless Mobile Syst.*, 2019.
- [12] P. Li and A. Aijaz, “Open RAN meets semantic communications: A synergistic match for open, intelligent, and knowledge-driven 6G,” in *Proc. IEEE Conf. Standards Commun. Netw.*, 2023.
- [13] C. Puligheddu, J. Ashdown, C. F. Chiasserini, and F. Restuccia, “SEM-O-RAN: Semantic O-RAN slicing for mobile edge offloading of computer vision tasks,” *IEEE Trans. Mob. Comput.*, vol. 23, no. 7, 2023.
- [14] E. Zeydan, L. Blanco, C. J. Vaca-Rubio, M. Caus, and K. Dev, “Semantic non-terrestrial communications with open ran-enabled 6G,” *IEEE Commun. Stand. Mag.*, 2025.
- [15] M. Elkael, M. Polese, R. Prasad, S. Maxenti, and T. Melodia, “ALL-STaR: Automated LLM-driven scheduler generation and testing for intent-based RAN,” *arXiv:2505.18389*, 2025.
- [16] H. Yin, P. Liu, K. Liu, L. Cao, L. Zhang, Y. Gao, and X. Hei, “ns3-ai: Fostering artificial intelligence algorithms for networking research,” in *Proc. ACM Wkshp. ns-3*, 2020, p. 57–64.
- [17] Y. Blau and T. Michaeli, “Rethinking lossy compression: The rate-distortion-perception tradeoff,” in *Proc. PMLR Int. Conf. Mach. Learn.*, 2019.
- [18] A. Radford, J. W. Kim, C. Hallacy, A. Ramesh, G. Goh, S. Agarwal, G. Sastry, A. Askell, P. Mishkin, J. Clark *et al.*, “Learning transferable visual models from natural language supervision,” in *Proc. PMLR Int. Conf. Mach. Learn.*, 2021.
- [19] Z. Wang, A. C. Bovik, H. R. Sheikh, and E. P. Simoncelli, “Image quality assessment: from error visibility to structural similarity,” *IEEE Trans. Image Process.*, vol. 13, no. 4, 2004.
- [20] J. Sneyers, “SSIMULACRA 2: Structural similarity unveiling local and compression related artifacts,” github.com/cloudinary/ssimulacra2, 2023, accessed: Jan. 2026.
- [21] 3GPP, “Evolved Universal Terrestrial Radio Access (E-UTRA); Physical layer procedures,” 3rd Generation Partnership Project (3GPP), Tech. Rep. ETSI TS 136 213, 2018.
- [22] H. Kellerer, U. Pferschy, and D. Pisinger, “Multidimensional knapsack problems,” in *Knapsack problems*. Springer, 2004.
- [23] 3GPP, “E-UTRA; User Equipment radio transmission and reception,” 3rd Generation Partnership Project (3GPP), Tech. Rep. ETSI TS 36.101, 2018.
- [24] ns-3 Project, “HybridBuildings Propagation Loss Model,” <https://www.nsnam.org>, ns-3 LTE Module Doc.
- [25] 3GPP, “Further Advancements for E-UTRA Physical Layer Aspects,” 3rd Generation Partnership Project (3GPP), Tech. Rep. TR 36.814, 2010.